A Statistical Model for Multiphoton Calcium Imaging of the Brain

Wasim Q. Malik, James Schummers, Mriganka Sur, and Emery N. Brown

Abstract— **Multiphoton calcium fluorescence imaging has gained prominence as a valuable tool for the study of brain cells, but the corresponding analytical regimes remain rather naive. In this paper, we develop a statistical framework that facilitates principled quantitative analysis of multiphoton images. The proposed methods discriminate the stimulus-evoked response of a neuron from the background firing and image artifacts. We develop a harmonic regression model with colored noise, and estimate the model parameters with computationally efficient algorithms. We apply this model to in vivo characterization of cells from the ferret visual cortex. The results demonstrate substantially improved tuning curve fitting and image contrast.**

I. INTRODUCTION

Multiphoton fluorescence imaging (MFI) has established itself as a valuable tool for real-time *in vivo* imaging of biological systems in the last decade [1]. It is the only technique that allows recording the activity of a large population of neurons simultaneously with subcellular resolution. A multiphoton microscope excites fluorophores in a biological sample using pulsed lasers, which leads to the emission of a fluorescence signal. A focussed laser beam is scanned in a raster pattern over a 2-D or 3-D region, producing an image typically spanning hundreds of cells. Highly informative and quantitative analyses related to a range of biological systems can thus be obtained from MFI data.

Besides other applications, MFI has been used for the characterization of brain structure and function [2]. Its ability to scan a large cell population enables us to map the neuronal and astrocytic network architectures [3], [4]. Its high spatial resolution can be used to study subcellular structures on the scale of dendritic spines [5], while its high temporal resolution allows the analysis of calcium waves and other cell and network dynamics [6]. With some post-processing, we can also obtain neuronal firing rate estimates comparable to those from electrophysiological recordings [7], [8].

The methods for the analysis of time series data generated from these calcium imaging datasets remain rudimentary.

Sophisticated signal processing and statistical modeling techniques are, however, required to extract maximum information from MFI data given its complexity. A number of artifacts that cause significant distortion to the data must also be modeled so that the true cell response can be recovered.

We develop a novel statistical signal processing framework for MFI data analysis in this paper, consisting of a harmonic signal model with colored noise similar to [9], and numerically efficient algorithms to estimate the parameters. We demonstrate the proposed methods with MFI data obtained from the ferret visual cortex as described below.

II. EXPERIMENTAL DESIGN

All experimental procedures followed have been approved by the MIT Committee on Animal Care, and adhere to the NIH guidelines for the Care and Use of Laboratory Animals.

A. Imaging

Multiphoton imaging of the fluorescent calcium indicator Oregon Green Bapta (OGB) was performed in the visual cortex of anesthetized ferrets, *in vivo*. Neurons were bulk-loaded with OGB by intracortical injection of the AM-ester conjugated form of OGB using standard techniques [3], [4], [10]. Imaging was performed with a custom-made multiphoton laser scanning microscope consisting of a modified Olympus Fluoview confocal scan head and a titanium/sapphire laser providing approx. 100 fsec. pulses at 80 MHz pumped by a 10 W solid-state source [11]. Fluorescence was detected using photomultiplier tubes in whole-field detection mode. A $20\times$, 0.95 NA lens was used. Image acquisition was accomplished using Fluoview software. Time series traces of images (XYT) with a field-of-view of approx. $250 \times 250 \ \mu m$ were collected at 1 Hz. The images were taken from cortical layer 2/3, which was readily distinguished from layer 1 on the basis of the relative density of astrocytes and neurons.

B. Visual Stimulation

Visual stimuli were delivered via a $17''$ LCD display placed 0.15 m away from the eyes of the animal. The stimuli were generated with the Matlab software package using the PsychoPhysics Toolbox [12]. The stimulation protocol consisted of square-wave gratings with 100% contrast which drifted at 3 Hz and rotated $10°$ every second (each data frame). Thus the stimulus rotates $360°$ in 36 sec. and the time series of the response of a neuron to this stimulus approximates a full orientation tuning curve. This stimulus was repeated three times to enhance the statistical reliability of the observations. Prior to recording these responses, 10 image frames were acquired in the absence of any visual stimulus to establish the baseline response level.

C. Image Pre-Processing

Image files collected by MFI were imported into Matlab and analyzed with custom routines. The cell bodies were identified by inspection and outlined manually. To avoid spillover from surrounding neuropil, which presumably contains indistinguishable processes of both astrocytes and neurons, conservative boundaries were defined. The relative fluorescence, $\Delta F_k = (F_k - F_0)/F_0$, was calculated, where F_k is the kth time-sample of the measured fluorescence intensity; F_0 is the baseline fluorescence; $k = 1, \ldots, K$; and K is the number of samples. Only cells with ΔF clearly distinguishable from the neuropil were chosen for subsequent analysis. Each pixel was treated independently, with each of its time-samples corresponding to a certain stimulus state.

III. MODELING AND ESTIMATION

Conventional approaches to modeling MFI data consist of averaging the measured fluorescence levels at an image pixel over multiple trials and smoothing across 2-D space and time. We adopt a generalized approach based on Fourier series expansion to model the tuning curves. Our goal here is to reliably separate the stimulus-dependent neuronal response from background activity, noise and other artifacts in the MFI time series data. It is therefore desirable to decompose the response data into a deterministic stimulus-evoked and a stochastic stimulus-free component, i.e.,

$$F_k = y_k = s_k + v_k. \tag{1}$$

Given the experimental conditions, we denote the periodic orientation stimulus with $\phi_k = 2\pi k/\tau_\phi$, where $\tau_\phi = 36$ sec. is the period. With this stimulus, a suitable set of basis functions to model the data can be defined in terms of a family of sinusoidal harmonics. Then, the stimulus-evoked response can be written in the form of a linear regression as

$$s_k = \mu + \sum_{h=1}^{H} \left\{ a_h \cos\left(h\phi_k\right) + b_h \sin\left(h\phi_k\right) \right\}, \tag{2}$$

where H denotes the number of harmonics included in the model, μ is the intercept, and a_h and b_h are the coefficients of the hth harmonic term. In accordance with Fourier theory, this sinusoidal basis can represent an arbitrary periodic function with the appropriate model order, H. In practice, many neurons and astrocytes, including those in V1, are known to have a sinusoidal tuning curve. This characteristic makes the model in (2) a natural choice, as a small H will suffice to adequately model the observed cellular response to ϕ.

The stochastic component, v_t, is a mixture of several noise processes. A pth order autoregressive model, $AR(p)$,

$$v_k = \sum_{m=1}^{p} c_m v_{k-m} + \epsilon_k, \tag{3}$$

can well approximate such a colored noise process. Here, c_m is the mth AR model coefficient with $m = 1, 2, \ldots, p$, and $\epsilon_k \sim \mathcal{N}(0, \sigma_\epsilon^2)$ represents a zero-mean, independently, identically distributed Gaussian process with variance σ_ϵ^2.

We can express this formalism using matrix notation as

$$\mathbf{y} = \mathbf{s} + \mathbf{v} = \mathbf{X}\theta + \mathbf{v}, \tag{4}$$

where $\mathbf{y} = [y_1, \ldots, y_K]^{\text{T}}$ are the measured fluorescence levels; $\mathbf{s} = [s_1, \ldots, s_K]^{\text{T}}$ and $\mathbf{v} = [v_1, \ldots, v_K]^{\text{T}}$ are the stimulus-evoked and stimulus-free components of $\mathbf{y}$; $\mathbf{X}$ is the regression design matrix containing the covariates in (2) including the intercept; $\theta = [\mu, a_1, b_1, \ldots, a_H, b_H]^{\text{T}}$ are the harmonic coefficients; $\psi = [c_1, c_2, \ldots, c_p]^{\text{T}}$ are the AR coefficients; $\varepsilon = [\epsilon_1, \epsilon_2, \ldots, \epsilon_K]^{\text{T}}$ is the noise vector; $\mathbf{v} \sim AR(0, \mathbf{\Gamma})$; and $\mathbf{\Gamma} = \mathcal{E}\left[(\mathbf{v} - \mathcal{E}\left[\mathbf{v}\right])(\mathbf{v} - \mathcal{E}\left[\mathbf{v}\right])^{\text{T}}\right]$.

The above formulation can be used to obtain best-fit estimates of the model parameters. We use ordinary least squares (OLS) estimation to obtain the estimates of the regression coefficients, given by [13]

$$\hat{\theta} = \left(\mathbf{X}^{\text{T}}\mathbf{X}\right)^{-1}\mathbf{X}^{\text{T}}\mathbf{y}. \tag{5}$$

The confidence intervals at a given confidence level are easily obtained for these estimates. For the ith coefficient, θ_i, approximate $P = 100(1-\alpha)\%$ confidence intervals are

$$\hat{\theta}_i - se_{\theta,i}\, t_{\alpha/2,d_\theta} \le \theta_i \le \hat{\theta}_i + se_{\theta,i}\, t_{\alpha/2,d_\theta}, \tag{6}$$

where t_{γ,d_θ} is the γth percentile point of the t distribution with $d_\theta = K - (2H + 1)$ degrees of freedom, and

$$se_{\theta,i} = \sqrt{(\mathbf{X}^{\text{T}}\mathbf{\Gamma}^{-1}\mathbf{X})_{ii}^{-1}}. \tag{7}$$

Based on these intervals, we can design the t-test for the significance of θ_i by defining the alternative hypothesis

$$H_1 : \quad \left|\frac{\hat{\theta}_i}{se_{\theta,i}}\right| > t_{\alpha/2,d_\theta}. \tag{8}$$

Thus θ_i makes a significant marginal contribution to the model if the null hypothesis is rejected.

Using these OLS coefficient estimates, we obtain the estimated stimulus-evoked response as $\hat{\mathbf{s}} = \mathbf{X}\hat{\theta}$. Its approximate $100(1-\alpha)\%$ confidence intervals are given by

$$\hat{s}_k - se_{s,k}\, t_{\alpha/2,d_\theta} \le s_k \le \hat{s}_k + se_{s,k}\, t_{\alpha/2,d_\theta} \tag{9}$$

where

$$se_{s,k} = \sqrt{\left(\mathbf{X}\left(\mathbf{X}^{\text{T}}\mathbf{\Gamma}^{-1}\mathbf{X}\right)^{-1}\mathbf{X}^{\text{T}}\right)_{kk}^{-1}}. \tag{10}$$

The residuals from the above OLS estimation procedure yield the $AR(p)$ process

$$\hat{\mathbf{v}} = \mathbf{y} - \hat{\mathbf{s}} = \mathbf{y} - \mathbf{X}\hat{\theta}. \tag{11}$$

The AR coefficient estimates, $\hat{\psi}$, of $\hat{\mathbf{v}}$, can be obtained by applying any of a number of well-known techniques, and the variance estimate, $\hat{\sigma}_\epsilon$, of the residual white noise, $\hat{\varepsilon} = \hat{\mathbf{v}} - \mathbf{V}\psi$, can be obtained similarly. The Burg algorithm, which provides least squares estimates of ψ by applying the Levinson-Durbin recursion, offers an efficient procedure. The approximate confidence intervals for AR coefficients are

$$\hat{\psi}_i - se_{\psi,i}\, t_{\alpha/2,d_\psi} \le \psi_i \le \hat{\psi}_i + se_{\psi,i}\, t_{\alpha/2,d_\psi}, \tag{12}$$

where $d_\psi = K - p$ are the degrees of freedom,

$$se_{\psi,i} = \sqrt{\hat{\sigma}_\epsilon^2 \left(\hat{\mathbf{V}}^\mathsf{T}\hat{\mathbf{V}}\right)_{ii}^{-1}}, \qquad (13)$$

is the standard error of the AR coefficient estimates, and

$$\hat{\mathbf{V}} = \begin{bmatrix} \hat{v}_{-1} & \cdots & \hat{v}_{-p} \\ \vdots & \ddots & \vdots \\ \hat{v}_{K-1} & \cdots & \hat{v}_{K-p} \end{bmatrix}. \qquad (14)$$

The corresponding t-test for the significance of the ith AR coefficient, ψ_i, is given by

$$H_1 : \quad \left| \frac{\hat{\psi}_i}{se_{\psi,i}} \right| > t_{\alpha/2, d_\psi}. \qquad (15)$$

The whiteness of AR residuals, $\hat{\epsilon}_k$, can be tested using the Ljung-Box portmanteau test, for which the test statistic is

$$Q = K(K+2) \sum_{\tau=1}^{T} \frac{r_\tau^2(\epsilon)}{K - \tau}, \qquad (16)$$

where $r_\tau(\epsilon) = d_\tau/d_0$ is the normalized autocovariance,

$$d_\tau = \frac{1}{K} \sum_{m=1}^{K-\tau} \left(\hat{\epsilon}_m - \bar{\epsilon}\right)\left(\hat{\epsilon}_{m+\tau} - \bar{\epsilon}\right) \qquad (17)$$

and $\bar{\epsilon} = \mathcal{E}[\hat{\epsilon}]$. The null hypothesis for the whiteness test is $H_0 : Q \sim \chi_{\alpha, T-p}^2$.

Thus, the estimates for the $2H + p + 2$ model coefficients, $\{\hat{\mu}, \hat{\theta}, \hat{\psi}, \hat{\sigma}_\epsilon\}$, are obtained. The stimulus-evoked response estimate, $\hat{s}_k$, can now be used to reconstruct denoised images.

IV. RESULTS

In this section, we apply the techniques developed in the previous section to the MFI data. The above model is applied to the fluorescence time series, $y_k = F_k$, obtained in response to the stimulus, ϕ_k, at each pixel in the 256×256 image. The estimates for the regression and AR coefficients, and the signal and noise components of the data, are obtained. No across-trial averaging or spatiotemporal smoothing is performed to prevent any loss of information. We empirically find that $H = 4$ and $p = 8$ provide good fits, and use these values in this analysis. In our future work, we will optimize the model orders by using the appropriate selection criteria.

As a representative example, Fig. 1(a) illustrates that the model provides a good fit, $\Delta\hat{y}_k$, to the measured relative fluorescence, ΔF_k. Quantitatively, the relative root mean square error is 7.8%. The AR process, v_k, in Fig. 1(b) captures the rest of the structure in the time series related to background firing, noise and other processes independent of the stimulus. From Fig. 1(c), the harmonic model provides a smooth estimate, $\Delta\hat{s}_k$, of the stimulus-evoked relative response and captures the complex shape of the tuning curve.

The whiteness analysis of the AR residuals, $\hat{\varepsilon}$, is important to ensure that they are i.i.d. and normal, which would indicate that the model is appropriate. Thus, in Fig. 2, we compare the quantiles of the residuals to the normal distribution, and
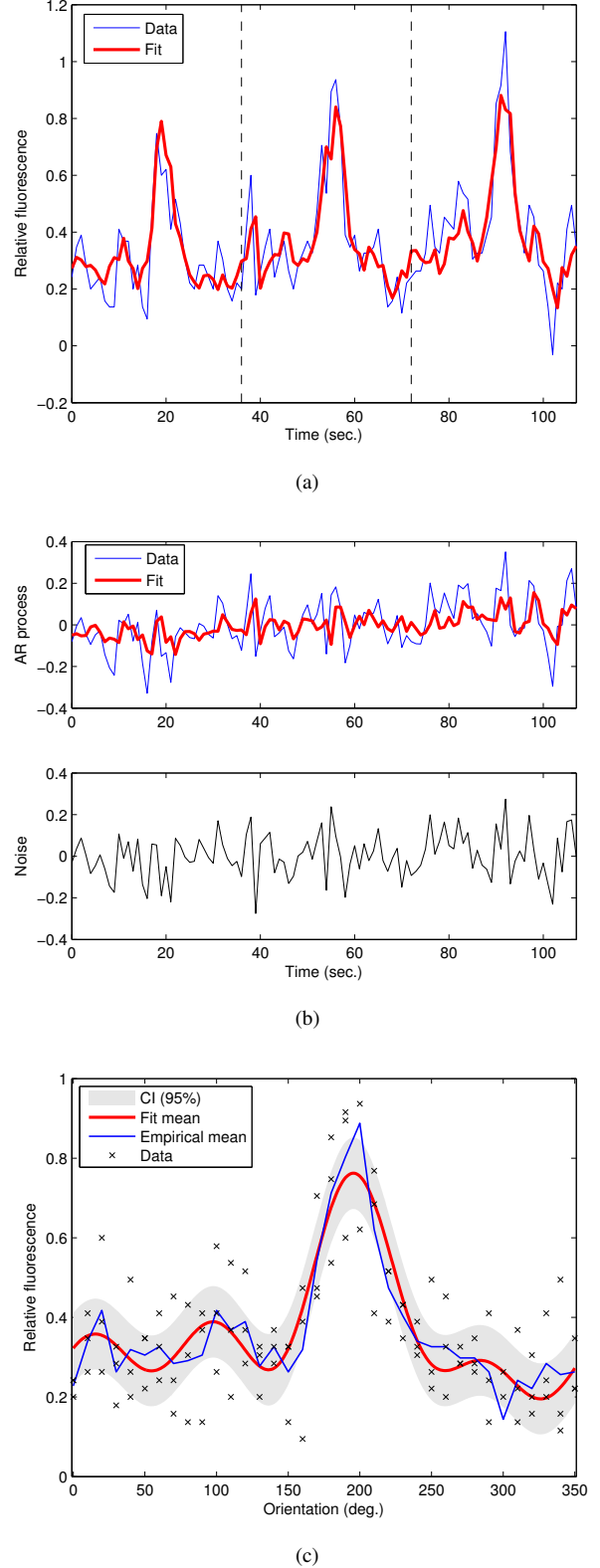

(a)

(b)

(c)

Fig. 1. Modeling the calcium fluorescence time series at an image pixel, relative to the baseline fluorescence obtained from measurements in the absence of the stimulus. (a) The recorded fluorescence, ΔF_k, over three full-cycle repetitions of the stimulus, along with the fit, $\Delta\hat{y}_k$, obtained with our signal-plus-noise model. (b) The AR process, v_k, and its fit, $\hat{v}_k$ (top), and the redisual white noise, $\hat{\epsilon}_k$ (bottom). (c) The response tuning curves obtained from the measured data by averaging over the three trials, and from the harmonic model, $\Delta\hat{s}_k$, with the approximate 95% confidence intervals.
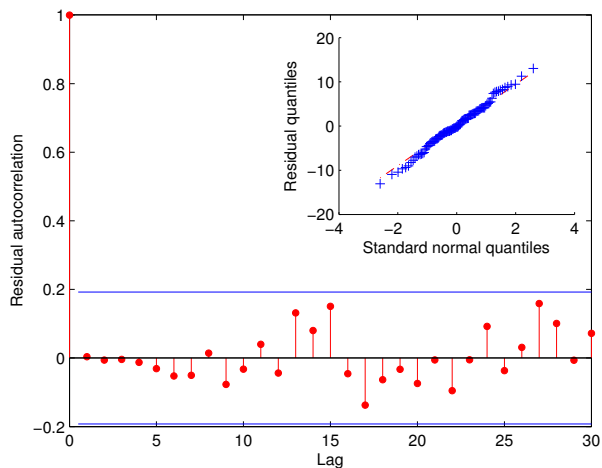
Fig. 2. Analysis of the statistical characteristics of the residual noise, ϵ_k, to determine its whiteness and normality. The autocorrelation function of the residuals is shown along with the 95% confidence intervals for up to 30 lags. The inset shows the quantile-quantile plot comparing the probability distribution of the residuals to a normal distribution.
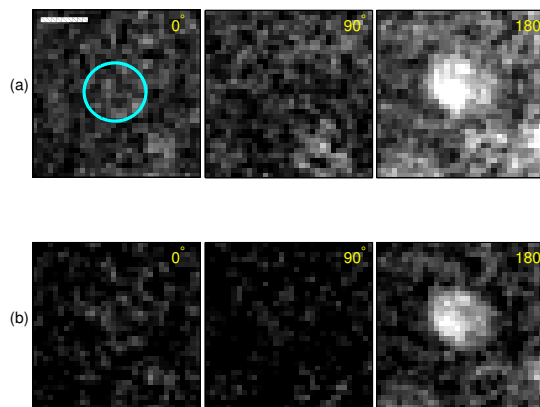

Fig. 3. Two-dimensional ΔF responses of a single cell at the specified orientation. (a) With conventional processing (averaging across trials). (b) The stimulus evoked response, $\hat{s}_k$, from the proposed model. The circle shows the location of the cell body identified manually, and the scale bar in (a) represents 10 μm. No spatial or temporal smoothing is applied in order to show the raw data. The brightness is scaled to represent $\Delta F = [0, F_{max}]$.

find only minor deviations at the tails. The sample autocorrelation function, $r_\tau(\epsilon)$, substantially resembles that of a white noise process within the 95% bounds given by $\pm 2/\sqrt{K}$. In addition, it is found that the residuals pass the Ljung-Box test (H_0). This implies that the AR process has satisfactorily captured the structure in the harmonic model's residuals, and all systematic variation in the data has been accounted for. The stimulus-evoked and stimulus-free response components have now been separated as desired. The former can be used in further analysis to model the neuronal response characteristics such as the orientation selectivity, preferred and non-preferred orientations, and tuning depth from $\Delta \hat{s}_k$.

It is also now straight-forward to reconstruct cellular or population images from $\hat{s}_k$ for each pixel. In Fig. 3, we compare the ΔF images of a cell obtained from our method with those obtained by conventional processing at some selected value of the orientation stimulus. Note from Fig. 1(c) that the maximum response of this cell occurs near $\phi = 180°$. Significantly enhanced contrast and noise suppression at both preferred and nonpreferred orientations is obtained after applying the proposed method, allowing us to observe the calcium dynamics in greater detail. This example demonstrates the superior denoising capability and signal-to-noise ratio improvement due to the proposed model.

V. CONCLUSION

We have presented a framework to model the time-series data obtained from high-resolution multiphoton imaging of live brain cells. The statistical model and algorithms for the analysis of calcium imaging data proposed in this paper are simple and efficient yet powerful and flexible. Separating the signal and noise components in the time series data for each pixel, our approach facilitates substantially improved characterization of neuronal response characteristics and denoising of cellular and population images. The framework presented in this paper can be easily extended to a broad class of imaging regimes with applications in biomedical systems and other areas in engineering.

REFERENCES

[1] W. Denk and K. Svoboda, "Photon upmanship: why multiphoton imaging is more than a gimmick," *Neuron*, vol. 18, no. 3, pp. 351–357, Mar. 1997.
[2] J. N. D. Kerr and W. Denk, "Imaging in vivo: watching the brain in action," *Nature Neuroscience*, vol. 9, no. 3, pp. 195–205, Mar. 2008.
[3] J. Schummers, H. Yu, and M. Sur, "Tuned responses of astrocytes and their influence on hemodynamic signals in the visual cortex," *Science*, vol. 320, no. 5883, pp. 1638–1643, Jun. 2008.
[4] K. Ohki, S. Chung, Y. H. Ch'ng, P. Kara, and C. R. Reid, "Functional imaging with cellular resolution reveals precise micro-architecture in visual cortex," *Nature*, vol. 433, no. 7026, pp. 597–603, Feb. 2005.
[5] A. Majewska and M. Sur, "Motility of dendritic spines in visual cortex in vivo: Changes during the critical period and effects of visual deprivation," *Proc. Natl. Acad. Sci.*, vol. 100, no. 26, pp. 16 024–16 029, Dec. 2003.
[6] W. Göbel, B. M. Kampa, and F. Helmchen, "Imaging cellular network dynamics in three dimensions using fast 3D laser scanning," *Nature Methods*, vol. 4, no. 1, pp. 73–79, Dec. 2006.
[7] E. Yaksi and R. W. Friedrich, "Reconstruction of firing rate changes across neuronal populations by temporally deconvolved Ca^{2+} imaging," *Nature Methods*, vol. 3, no. 5, pp. 377–383, May 2006.
[8] D. S. Greenberg, A. R. Houweling, and J. N. D. Kerr, "Population imaging of ongoing neuronal activity in the visual cortex of awake rats," *Nature Neuroscience*, vol. 11, no. 7, pp. 749–751, Jul. 2008.
[9] E. N. Brown, Y. Choe, H. Luithardt, and C. A. Czeisler, "A statistical model of the human core-temperature circadian rhythm," *Am. J. Physiol. Endocrinol. Metab.*, vol. 279, no. 3, pp. E669–E683, Sep. 2000.
[10] C. Stosiek, O. Garaschuk, K. Holthoff, and Konnerth, "In vivo two-photon calcium imaging of neuronal networks," *Proc. Natl. Acad. Sci.*, vol. 100, no. 12, pp. 7319–7324, Jun. 2003.
[11] A. Majewska, G. Yiu, and R. Yuste, "A custom-made two-photon microscope and deconvolution system," *Eur. J. Physiol.*, vol. 441, no. 2-3, pp. 398–408, Dec. 2000.
[12] D. H. Brainard, "The psychophysics toolbox," *Spatial Vision*, vol. 10, no. 4, pp. 433–436, 1997.
[13] D. C. Montgomery, C. L. Jennings, and M. Kulahci, *Introduction to Time Series Analysis and Forecasting*. Wiley, 2008.